High-spin spectroscopy of ^{109}Te

Zs. Dombrádi,[1] B. M. Nyakó,[1] G. E. Perez,[1] A. Algora,[1] C. Fahlander,[2] D. Seweryniak,[2,10] J. Nyberg,[2] A. Atac,[2] B. Cederwall,[3] A. Johnson,[3] A. Kerek,[3] J. Kownacki,[4] L-O. Norlin,[3] R. Wyss,[3] E. Adamides,[5] E. Ideguchi,[6] R. Julin,[7] S. Juutinen,[7] W. Karczmarczyk,[10] S. Mitarai,[6] M. Piiparinen,[7] R. Schubart,[8,11] G. Sletten,[9] S. Törmänen,[7] and A. Virtanen[7]

[1] *Institute of Nuclear Research of the Hungarian Academy of Sciences, Debrecen, Hungary*
[2] *The Svedberg Laboratory and Department of Radiation Sciences, Uppsala University, Uppsala, Sweden*
[3] *Department of Physics, The Royal Institute of Technology, Stockholm, Sweden*
[4] *Heavy Ion Laboratory, University of Warsaw, Warsaw, Poland*
[5] *National Centre for Scientific Research, Ag. Paraskevi, Attiki, Greece*
[6] *Department of Physics, Faculty of Science, Kyushu University, Fukuoka, Japan*
[7] *Department of Physics, University of Jyväskylä, Jyväskylä, Finland*
[8] *Hahn-Meitner Institut, Berlin, Germany*
[9] *The Niels Bohr Institute, University of Copenhagen, Copenhagen, Denmark*
[10] *Institute of Experimental Physics, University of Warsaw, Warsaw, Poland*
[11] *II. Physikalisches Institut, Universität Göttingen, Germany*

(Received 22 December 1994)

Excited states of the neutron deficient nucleus ^{109}Te were identified for the first time in the ^{54}Fe(^{58}Ni,2pn) reaction by in-beam γ-spectroscopic methods. The NORDBALL detector array, equipped with a charged-particle and a neutron detector system for reaction channel identification, was used to detect the evaporated particles and γ rays. A level scheme was constructed on the basis of $\gamma\gamma$-coincidence relations, and the angular momenta of the states were determined from the measured angular correlation intensity ratios. Two favored bands built on the $\nu g_{7/2}$ and $\nu h_{11/2}$ neutron quasiparticle states were identified. The structure of the nucleus is discussed in the framework of the particle-vibration coupling model using the interacting boson-fermion formalism up to spin 27/2. The negative parity sequence is compared to Total Routhian Surface calculations.

PACS number(s): 23.20.Lv, 25.70.Gh, 27.60.+j, 21.60.Ev

I. INTRODUCTION

A great interest is shown in the identification and study of the structure of nuclei close to the proton drip line. One of the long-standing problems in the study of exotic nuclei is to reach the doubly magic nucleus ^{100}Sn. Nuclei far from the stability line are produced with very low cross sections in heavy-ion reactions. Therefore in their identification the use of highly efficient and sensitive techniques is required. In an experiment performed at NORDBALL, several of very neutron deficient nuclei were identified in beam in the $A \approx 100$ region [1] for the first time. As a result of this experiment also the level schemes of three light Te isotopes, ^{108,109,110}Te, for which practically only the ground states were known earlier, have been deduced [2,3]. In this work we report results on the structure of ^{109}Te.

The nucleus ^{109}Te was previously investigated in β-decay and in β-delayed proton- and α-decay studies [4]. In these experiments only the half-life of the ground state was determined. The aim of the present work was to get information on the excited states of ^{109}Te using in-beam spectroscopic methods. To interpret the experimentally observed states of this nucleus the interacting boson-fermion model was applied. High-spin states are compared to deformed mean-field calculations, based on the cranked Strutinsky approach.

II. EXPERIMENTAL METHODS AND RESULTS

In the experiment a 10 mg/cm^2 thick ^{54}Fe target isotopically enriched to 99.8% was bombarded with a 270 MeV ^{58}Ni beam from the accelerator facilities of the Niels Bohr Institute. The particles and γ rays emitted from the ^{112}Xe compound nucleus were detected with the NORDBALL detector system [5], which was set up with 15 BGO-shielded Ge detectors and with a 30-element γ-ray calorimeter of BaF_2 crystals covering the backward 2π hemisphere. The detector system was further equipped with 11 liquid scintillator detectors of about 1π solid angle in the forward direction [6] to detect neutrons, and with an inner 4π charged-particle detector array of 21 ΔE-type Si detectors [7] to give information on the number of emitted protons and α particles. The trigger condition was set to detect at least two γ rays in the calorimeter and at least two γ rays in the Ge detectors. Both neutron time-of-flight and pulse shape discrimination were used for neutron-γ discrimination.

A total of about 420×10^6 coincidence events were collected and then sorted into a set of E_γ-E_γ matrices by requiring different conditions on the number of detected charged particles and neutrons. In spite of the applied conditions, these matrices contained γ rays from several final nuclei, because some of the emitted particles have been undetected or misidentified. The γ rays of the ^{109}Te

nucleus appeared in the $1p$- and $2p$-, as well as in the $1n$-, $1p1n$-, and $2p1n$-gated matrices. The number of ^{109}Te γ rays collected into the $1p$- and $2p$-gated matrices was about a factor of 3 larger than in the $1n$-gated matrices due to the $\approx$25% efficiency of the neutron ball. The spectra obtained from these matrices were, however, of lower quality, as the high background originating from γ rays of nuclei produced without the emission of neutrons obscured the weak transitions of ^{109}Te. Thus in the data analysis the sum of the $1n$-, $1p1n$-, and $2p1n$-gated matrices was used. The contaminating γ lines of other nuclei present in this matrix due to undetected protons, neutrons, or α particles from reactions with higher particle multiplicities were eliminated by using a successive matrix subtraction technique. Finally some small corrections were made to remove transitions present because of identifying α particles as protons and to remove transitions from target and projectile excitations. The total projection spectrum of the cleaned matrix obtained in this way is shown in Fig. 1, where all labeled γ rays belong to ^{109}Te.

To confirm the assignment of the γ rays to ^{109}Te we used the raw matrices. By determining the intensity ratios of the γ rays in the spectra generated from matrices corresponding to different numbers of detected neutrons and protons, and comparing them with values obtained for known nuclei, one can unambiguously assign the reaction channel [1]. From the measured intensity ratios, the strongest γ rays in Fig. 1 were assigned to the reaction channel with the emission of two protons and one neutron leading to the nucleus ^{109}Te.

Standard gating techniques were used on the cleaned matrix, and all the coincidence relations were also checked in the original $p1n$-gated matrix. The energies and intensities of the γ rays assigned to ^{109}Te are summarized in Table I. They were deduced from the total projection spectrum and from the gated spectra. The relatively large errors of the intensities are due to the estimated systematic uncertainty coming from the matrix subtraction. Typical gated spectra of the pure ^{109}Te matrix are shown in Fig. 2.

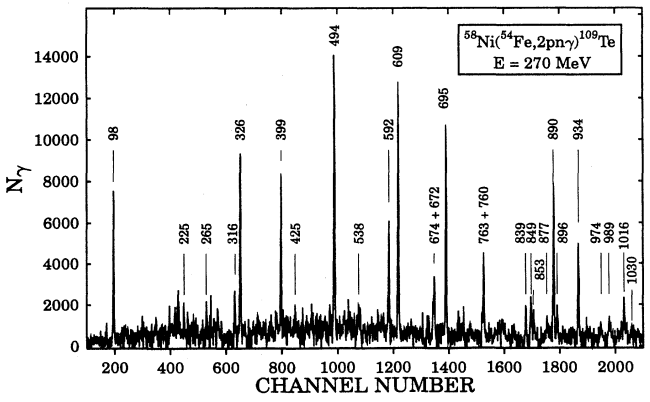

FIG. 1. Total projection spectrum of ^{109}Te obtained from the summed $1n$-, $1p1n$-, and $2p1n$-gated $\gamma\gamma$ matrix after the subtraction of the contaminating channels.

TABLE I. Energies, relative intensities, angular correlation intensity ratios, and angular momentum transferred by the γ-ray transitions assigned to ^{109}Te. Suggested spins and parities of the initial and final states of the transitions are given in the last column.

E_γ (keV)	I_γ (relative)	$\frac{I_\gamma(143°)}{I_\gamma(79°)+I_\gamma(101°)}$	ΔI ($\hbar$)	$I_i^\pi \rightarrow I_f^\pi$
98.1(1)	46(15)	0.99(13)	1	$(7/2_1^+) \rightarrow (5/2_1^+)$
224.6(5)	5(2)			$(9/2_2^+) \rightarrow (7/2_2^+)$
265.2(5)	5(2)			$(5/2_2^+) \rightarrow (5/2_1^+)$
316.2(2)	11(2)	1.65(67)		$(11/2_1^-) \rightarrow (11/2_1^+)$
326.1(1)	51(5)	0.75(10)	1	$(11/2_1^-) \rightarrow (9/2_2^+)$
398.7(1)	41(4)	0.80(12)	1	$(11/2_1^-) \rightarrow (9/2_1^+)$
424.5(5)	6(3)			$(9/2_1^+) \rightarrow (5/2_2^+)$
494.3(1)	100	1.47(22)	2	$(15/2_1^-) \rightarrow (11/2_1^-)$
537.6(5)	5(2)			$(7/2_2^+) \rightarrow (5/2_1^+)$
591.9(1)	40(4)	0.94(17)	1	$(9/2_1^+) \rightarrow (7/2_1^+)$
609.0(1)	99(9)	1.57(19)	2	$(19/2_1^-) \rightarrow (15/2_1^-)$
672.0(4)	13(2)	1.22(51)		$(37/2_1^-) \rightarrow (35/2_2^-)$
674.2(2)	28(5)	1.61(29)	2	$(11/2_1^+) \rightarrow (7/2_1^+)$
695.2(1)	96(9)	1.57(20)	2	$(23/2_1^-) \rightarrow (19/2_1^-)$
760.1(3)	15(4)	1.43(40)	(2)	$(15/2_1^+) \rightarrow (11/2_1^+)$
763.0(2)	44(6)	1.51(25)	2	$(9/2_2^+) \rightarrow (5/2_1^+)$
839.3(3)	15(5)	0.84(23)	1	$(37/2_1^-) \rightarrow (35/2_1^-)$
848.7(2)	17(5)	1.46(39)	(2)	$(35/2_1^-) \rightarrow (31/2_1^-)$
853.3(5)	9(2)	1.48(48)		
877.0(4)	14(4)	1.63(47)	(2)	$(33/2_1^-) \rightarrow (29/2_1^-)$
889.5(1)	88(8)	1.47(19)	2	$(27/2_1^-) \rightarrow (23/2_1^-)$
895.9(1)	20(4)	1.00(39)	(1)	$(29/2_1^-) \rightarrow (27/2_1^-)$
933.9(1)	61(6)	1.60(24)	2	$(31/2_1^-) \rightarrow (27/2_1^-)$
974.2(3)	7(3)	0.95(35)	(1)	
989.0(3)	16(3)	1.21(35)		
1015.9(2)	28(5)	1.88(41)	2	$(35/2_1^-) \rightarrow (31/2_1^-)$
1029.5(5)	6(3)	0.98(37)	(1)	

For most of the transitions $\gamma\gamma$ angular correlation intensity ratios were determined from the γ-ray intensities measured at $\approx$ 143° and $\approx$ 79°, 101° relative to the beam direction using the strong 494- and 98-keV transitions as gating transitions. The intensity ratios $R = \frac{I_\gamma(143°)}{I_\gamma(79°)+I_\gamma(101°)}$ shown in Table I were used to determine the angular momentum transferred by the γ rays. In the case of weak transitions the ratios R had too large errors to draw definite conclusions. Even in the case of strong transitions there remains some ambiguity, as the same ratio can correspond to, e.g., a $\Delta I = 2$ stretched $E2$ or a $\Delta I = 0$ mixed $M1/E2$ transition with appropriate mixing ratio, or similarly, the ratio can be the same for a pure $\Delta I = 0$ and a mixed $\Delta I = 1$ transition. In the analysis we always assumed $\Delta I > 0$. According to theoretical estimates for stretched $E2$ transitions $R \approx 1.5$ and for stretched dipole transitions $R \approx 0.8$.

The level scheme of ^{109}Te shown in Fig. 3 was constructed mainly on the basis of the coincidence relations and on the energy and intensity balances. The γ lines from the four lowest-lying states of the negative parity band have nearly equal intensities. Their ordering is based on the assumption that they form a quasirotational band. The order of the higher-lying transitions is well established by the coincidence and intensity rela-

tions. For the positive parity band, the order of the γ rays is determined by the intensity relations. The order of the 326- and 763-keV and the 399- and 592-keV lines, having nearly the same intensities, is also supported by the presence of the weak branches (225, 538 keV and 425, 265 keV). In these two weak branches the more intense γ rays in the gates corresponding to higher-lying γ rays were placed at higher energy. The summed intensity of the 316-, 326-, and 399-keV γ rays equals the intensity of the 494-keV transition, and so it seems that there is very little side feeding into the 1089-keV $(11/2^-)$ state.

The ground state of ^{109}Te was assigned as $I^\pi = 5/2^+$ on the basis of systematics of light $N = 57$ nuclei [8,9]. After that the spin values assigned to the excited states were mainly obtained from the measured angular correlation intensity ratios. The 98-keV ground state transition and the 592-keV transition have $\Delta I = 1$ character and thus suggest spin 7/2 and 9/2, respectively, for their initial states. Positive parity is proposed on the basis of expectations from the above mentioned systematics. Similarly, the 763-keV ground state transition is most likely a stretched $E2$, which suggests spin 9/2 and positive parity for its initial state. Both the 326- and the 399-keV transitions have small angular correlation intensity ratios ($\approx$0.8), consistent with stretched dipoles, indicating that the 1089-keV state has spin 11/2. We have assigned negative parity to this state on the basis of systematics. The spin values of the negative parity band are well established up to spin 35/2 by stretched $E2$ transitions. The large error in the angular correlation intensity ratios of the weaker transitions does not allow for precise spin assignments for the higher-lying states. The spin values in the sideband above 4673 keV came from the dipole nature of the interband and quadrupole character of the intraband transitions. The two lowest-lying transitions of the positive parity side band have stretched quadrupole character, suggesting 11/2 and 15/2 spin to their initial states. The 11/2 spin assignment to the 772-keV level is in agreement also with the angular correlation intensity ratios for the 316-keV and 674-keV transitions. The spin assignment of the states at 538 and 265 keV is proposed on the basis of theoretical considerations.

The positive parity band is yrast up to spin 15/2, even though it is not highly excited and weakly populated. This is because most of the feeding is gathered above spin 23/2 by the negative parity band, and there is no mixing between the two bands due to their different parities.

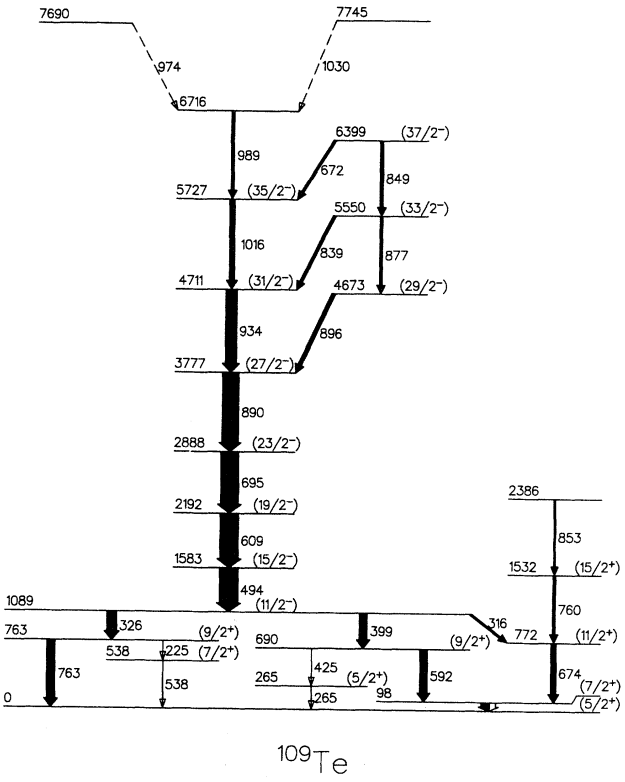

FIG. 3. Proposed level scheme of ^{109}Te from the ^{54}Fe(^{58}Ni,$2pn\gamma$)^{109}Te reaction. All the spin values are tentative, and they are given relative to the assumed ground state $I^\pi = 5/2^+$. The unfilled part of the 98 keV arrow represents the intensity of the conversion electrons, assuming pure $M1$ multipolarity.

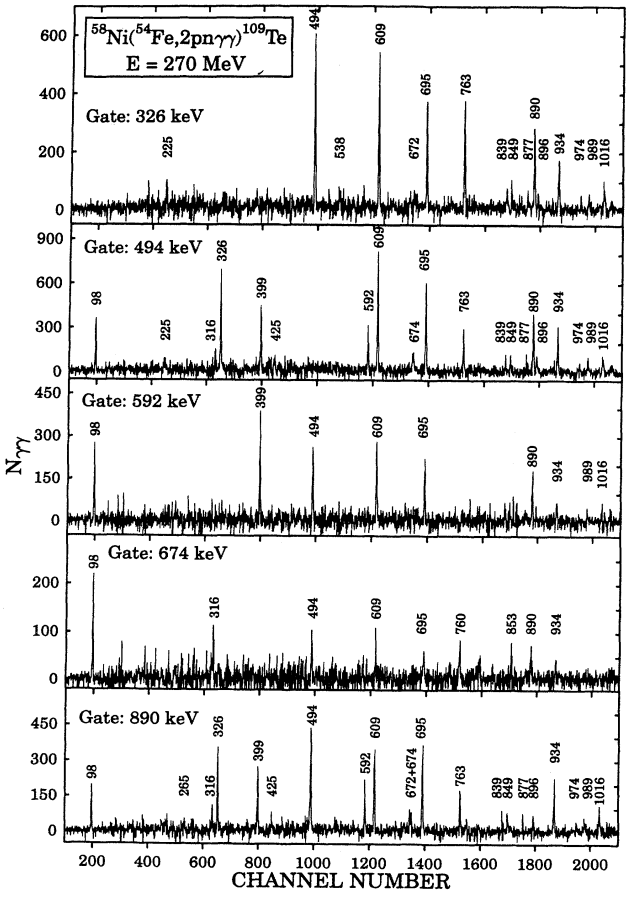

FIG. 2. Typical $\gamma\gamma$-coincidence spectra obtained from gates set on the cleaned matrix.

III. DISCUSSION

On the basis of the systematics of light $N = 57$ nuclei [8,9] low-lying $d_{5/2}$, $g_{7/2}$, and $h_{11/2}$ quasineutron states and vibrational bands built on them are expected to dominate the low energy part of the spectrum. To make these expectations more quantitative we calculated the structure of ^{109}Te in the vibrational limit of the interacting boson fermion model (IBFM).

The Hamiltonian of the interacting boson-fermion model is [10]

$$H_{\mathrm{IBFM}} = H_{\mathrm{IBM}} + H_{\mathrm{qp}} + H_{\mathrm{mon}} + H_{\mathrm{Qq}} + H_{\mathrm{exc}},$$

where H_{IBM} is the Hamiltonian of the interacting boson model [11], H_{qp} is the spherical quasiparticle Hamiltonian of the odd neutron, and H_{mon}, H_{Qq}, and H_{exc} denote the monopole, quadrupole, and exchange parts of the particle-vibration interaction, respectively.

The boson core was treated in the SU(5) limit of the IBM, adequate for vibrational nuclei. The maximum number of bosons was 4, corresponding to the four valence nucleon pairs of the ^{108}Te core. The d-boson (phonon) energy E_d and the hexadecapole boson-boson interaction strength C_4, describing to what extent the 4_1^+ state is pushed up relative to the energy $2E_d$, were determined by adjusting them to the spectrum of ^{108}Te [2], resulting in $E_d = 0.62$ MeV and $C_4 = 0.15$ MeV. The parameter χ describing the static part of the quadrupole moment of the d boson was deduced from the $B(E2; 2_1^+ \rightarrow 0_1^+)$ and $Q_{2_1^+}$ values of the ^{122,124}Te nuclei to be $\chi = -1.0$.

The shell model space consisted of the $s_{1/2}$, $d_{3/2}$, $d_{5/2}$, $g_{7/2}$, and $h_{11/2}$ subshells. The occupation probabilities were estimated in the BCS model using the Kisslinger-Sorensen parametrization [12]. The following values were adopted: $V^2(s_{1/2}) = 0.17, V^2(d_{3/2}) = 0.05, V^2(d_{5/2}) = 0.59, V^2(g_{7/2}) = 0.28$, and $V^2(h_{11/2}) = 0.06$. The relevant quasiparticle energies relative to the $d_{5/2}$ state were 0.11 MeV for the $g_{7/2}$ and 1.4 MeV for the $h_{11/2}$ orbital, obtained from the BCS calculations.

The boson-fermion coupling strengths were fitted to the energies of the positive parity states of ^{109}Te. The monopole interaction strength was 35 keV, which is a typical value in this mass region. The quadrupole-quadrupole interaction strength was 380 keV, which corresponds to a weak particle-vibration coupling. The strength of the exchange interaction, which takes into account the microscopic structure of the phonon and in this way simulates the Pauli principle, was 800 keV.

The calculated and measured level energies are compared in Fig. 4, where also the main configurations of the calculated states are given. There is a good correspondence between the calculated and experimental energies.

According to the calculations the ground state is the $d_{5/2}$ quasineutron state, and the first excited state is the $g_{7/2}$ neutron excitation. Its low energy is in agreement with the BCS calculations and also with the systematics in the sense that in the $N = 59$ nuclei the $7/2^+$ state become the ground state. The two $9/2^+$ states are the $9/2$ members of the $d_{5/2} \oplus 2_1^+$ and $g_{7/2} \oplus 2^+$ one-phonon

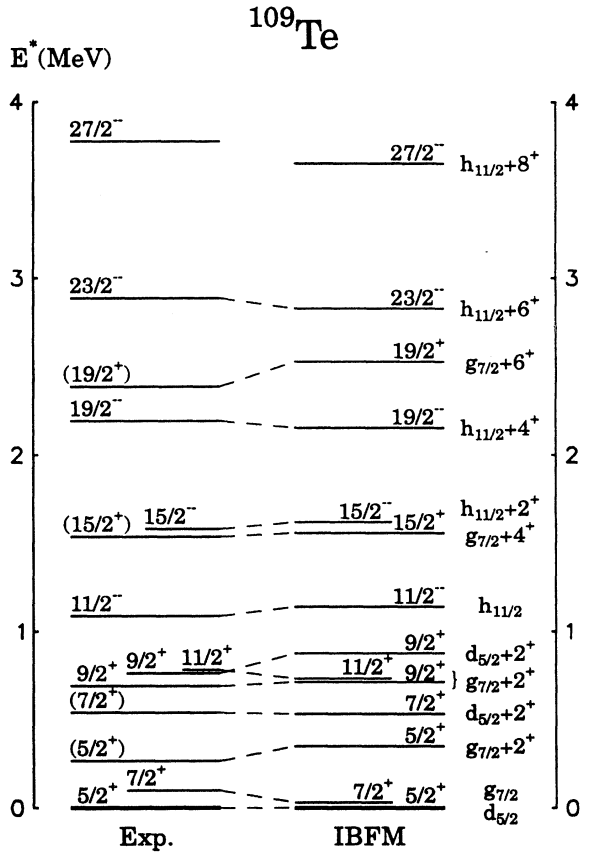

FIG. 4. Comparison of the experimental level scheme with the theoretical calculations based on the interacting boson-fermion model. On the right hand side of the figure the main components of the calculated wave functions are also given.

multiplets, while higher-spin positive parity states have mainly $g_{7/2} \oplus 2^+, 4^+, 6^+$ configurations. The negative parity states arise from the coupling of the $h_{11/2}$ neutron states to the yrast states of the ^{108}Te nucleus [2].

It is interesting to compare the vibrational bands built on the $7/2^+$ and $11/2^-$ states. The energy of the ΔI=2 γ rays, taking away one phonon energy from the system, is consistently lower with about 160 keV in the negative parity band than in the positive parity one. As both sets of states were interpreted as a quasiparticle coupled to the yrast states of ^{108}Te, a possible explanation may be that the high-j intruder $h_{11/2}$ neutron increased the moment of inertia (the average deformation) of the soft Te core by polarization. On the other hand, the IBFM describes well this difference, but cannot account for polarization phenomena. According to these calculations the way of particle-vibration coupling changed. In this model, as in all relevant particle-vibration coupling models, the particle is coupled to the core via the conventional quadrupole-quadrupole interaction, and via the exchange interaction, which is applied to describe the so-called $j - 1$ effect [13]. The effective strength of the quadrupole-quadrupole interaction is proportional to $(U^2 - V^2)$, while that for the exchange interaction is ap-

proximately proportional to UV. Thus, in the case of the nearly empty $\nu h_{11/2}$ quasiparticle state the quadrupole-quadrupole coupling is dominant, while in the case of the much more filled $\nu g_{7/2}$ quasiparticle state the exchange force also plays a significant role. This difference was enough to describe the above mentioned energy difference in the two bands.

The highest spin expected in the IBFM is 27/2, as the core has eight valence particles enough for four phonons. However, the negative parity band is not terminated at $27/2^-$. The classical way to investigate the nature of the high-spin states is based on the analysis of the spin along the rotational axis, $I_x = \sqrt{(I+1/2)^2 - K^2}$, as a function of the rotational frequency ($\hbar\omega \approx E_\gamma/2$). Such a plot is shown in Fig. 5. The experimentally extracted spin I_x is compared to cranked Strutinsky calculations, which are based on the deformed Woods-Saxon potential (we refer the reader to Refs. [14,15]). Within the mean field concept, there is no *a priori* limit of the spin, which is calculated microscopically, via the summed contributions of all quasiparticles.

In the cranking model the first $\nu h_{11/2}$ crossing is blocked, due to the occupation of that orbital. The small increase in angular momentum at $\hbar\omega \approx 0.45$ MeV coincides with the calculated alignment of $g_{7/2}$ neutrons. In addition there is a smooth alignment due to $g_{7/2}$ protons, with a very large interaction (Fig. 5). The total calculated angular momentum is, however, smaller by $\approx 2\hbar$ than the experimental one. A possible mechanism for this discrepancy might be related to the vibration-rotation coupling, which is beyond the scope of the cranking model. The coupling to, e.g., one aligned quadrupole phonon might thus be responsible for the above discrepancy.

At even higher frequency, $\hbar\omega = 0.5$ MeV, a pronounced angular momentum increase is present in the data (Fig. 5). In the even-even isotope ^{112}Te, a nice rotational band has been observed, based upon the proton $h_{11/2}$ intruder orbital [16]. In our calculations, one expects a crossing with the $\pi(h_{11/2})^2$ band to occur around $\hbar\omega \approx 0.6$ MeV. At that frequency, one also expects the first unblocked $h_{11/2}$ neutron crossing. Protons as well as neutrons occupying the $h_{11/2}$ orbital strongly polarize the quadrupole deformation to larger values (from $\beta_2 = 0.14$, $\gamma = 15°$ to $\beta_2 = 0.22$, $\gamma = 10°$). The alignment gain at $\hbar\omega = 0.5$ MeV might thus be interpreted as a crossing with the more deformed $\pi(h_{11/2})^2 - \nu(h_{11/2})^3$

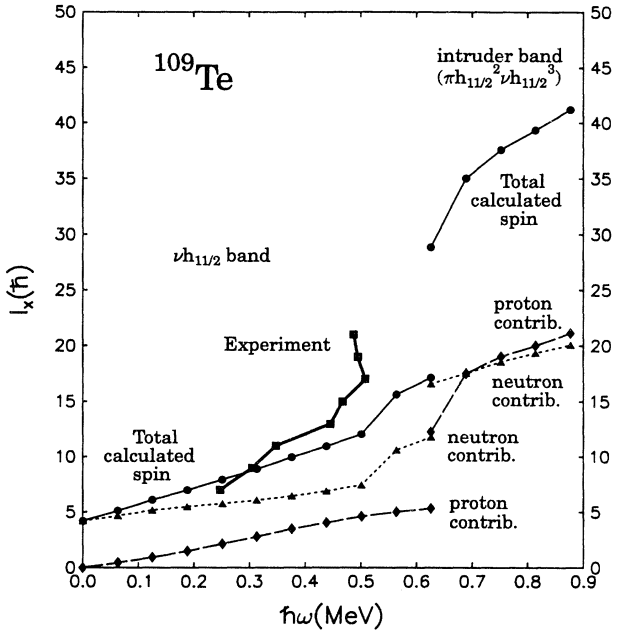

FIG. 5. Experimental and calculated spin I_x for the observed negative parity band.

configuration. A comparison of that crossing with the one in the intruder band of the even-even Te isotopes yields that it takes place later in the calculations than in the experiment. Since, however, the present data are not followed to higher-spin values, one has to be careful with a definite assignment, and the discussion of the possible alignment at $\hbar\omega = 0.5$ MeV is therefore somewhat speculative.

ACKNOWLEDGMENTS

This work was supported by the Danish, Finnish and Swedish Natural Science Research Councils, the Hungarian Fund for Scientific Research (OTKA Contract No. T7481), and the Polish Scientific Research Committee. In the data analysis a program package by D. C. Radford was partly applied.

[1] A. Johnson *et al.*, in Proceedings of the International Conference on Rapidly Rotating Nuclei, Tokyo, 1992 [Nucl. Phys. **A557**, 401c (1993)]; D. Seweryniak *et al.*, in Proceedings of the International Conference on Nuclear Structure at High Angular Momentum, Ottawa, 1992, Report No. AECL-10613 (unpublished), Vol. 2, p. 449.
[2] Zs. Dombrádi *et al.*, Z. Phys. A **350**, 3 (1994).
[3] C. Fahlander *et al.*, Nucl. Phys. **A577**, 773 (1994).
[4] J. Blachot, Nucl. Data Sheets **64**, 913 (1991).
[5] B. Herskind, Nucl. Phys. **A447**, 395 (1985); G. Sletten, in *Proceedings of the International Seminar on Frontier of Nuclear Spectroscopy*, Kyoto, 1992, edited by Y. Yoshizawa, H. Kusakari, and T. Otsuka (World Scientific, Singapore, 1993).
[6] S. E. Arnell, H. A. Roth, Ö. Skeppstedt, J. Bialkowski, M. Moszynski, D. Wolski, and J. Nyberg, Nucl. Instrum. Methods A **300**, 303 (1991).
[7] T. Kuroyanagi, S. Mitarai, S. Suematsu, B. J. Min, H. Tomuza, J. Mukai, T. Maeda, R. Nahatani, G. Sletten, J. Nyberg, and D. Jerrestam, Nucl. Instrum. Methods A

316, 289 (1992).
[8] D. De Frenne and E. Jacobs, Nucl. Data Sheets **68**, 935 (1993).
[9] D. De Frenne, E. Jacobs, M. Verboven, and P. De Gelder, Nucl. Data Sheets **47**, 261 (1986).
[10] F. Iachello and O. Scholten, Phys. Rev. Lett. **43**, 679 (1979); V. Paar, S. Brant, L. F. Canto, G. Leander, and M. Vouk, Nucl. Phys. **A378**, 41 (1982).
[11] A. Arima and F. Iachello, Phys. Rev. Lett. **35**, 1069 (1975); D. Janssen, R. V. Jolos, and F. Dönau, Nucl. Phys. **A224**, 93 (1974).
[12] L. S. Kisslinger and R. A. Sorensen, Rev. Mod. Phys. **35**, 853 (1963).
[13] F. Dönau and D. Janssen, Nucl. Phys. **A209**, 109 (1973).
[14] R. Wyss, J. Nyberg, A. Johnson, R. Bengtsson, and W. Nazarewicz, Phys. Lett. B **215**, 211 (1988); Z. Phys. A **329**, 255 (1988).
[15] W. Nazarewicz, R. Wyss, and A. Johnson, Phys. Lett. B **225**, 208 (1989).
[16] E. S. Paul *et al.*, Phys. Rev. C **50**, 698 (1994).